National Conference with International Participation
ENGINEERING MECHANICS 2007
Svratka, Czech Republic, May 14 – 17, 2007

MODELING OF REINFORCEMENT CORROSION IN CONCRETE

D. Matesová, M. Vořechovský [1]

Summary: *Corrosion of reinforcing steel in concrete is one of the most influencing factors causing the degradation of reinforced concrete structures, conducting to concrete cracking and spalling. The detrimental effect of corrosion is due to the fact that a rust product has a volume 2 - 6 times larger than the original steel. Consequently, the rust products exert an expansive stress on the surrounding concrete whose tensile strength is usually low. This paper attempts the application of an analytical and numerical approaches to simulation of concrete cracking due to corrosion of reinforcement. At first, a combination and detailed analysis of two analytical models proposed by Liu and Weyers (1998) and Li et al. (2006) is presented. Four distinct phases of the corrosion process are identified and a detailed guide through the mathematical development is described. In the next, numerical computations obtained with nonlinear finite element code are presented. The model features the state-of-the-art in nonlinear fracture mechanics modeling and the heterogeneous structure of concrete is modeled via spatially varying parameters of the constitutive law. The crack growth in concrete induced by corrosion of steel reinforcement is modeled with the crack band model combined with a suitable damage law. Finally, the results of the analytical studies are compared to numerical computations obtained with the nonlinear finite element code and the paper concludes with a real-life numerical example.*

1. Introduction

Corrosion of reinforcement embedded in concrete is an electrochemical process during which coupled anodic and cathodic reactions take place. Pore water acts as an electrolyte. The detrimental effect of corrosion is due to the fact that a rust product has a volume 2 - 6 times larger than the original steel. Consequently, it causes volume expansion, developing tensile stress in the surrounding concrete. Reinforcement corrosion takes place during the propagation period, and its rate is governed by the availability of water and oxygen on the steel surface. Due to corrosion, the effective area of the steel decreases and rust products grow, causing, at a certain stage, longitudinal cracking, and later, the spalling of concrete cover (delamination). Generally two types of corrosion are distinguished: the *uniform* (or general) type and the *pitting* (localized) type of corrosion. The subject of this paper is the uniform type of corrosion.

In this paper, a combination and detailed analysis of the two analytical models proposed earlier is presented. Next, numerical computations obtained with nonlinear finite element code

[1] Ing. Dita Matesová, Ph.D., Ing. Miroslav Vořechovský, Ph.D., Institute of Structural Mechanics, Faculty of Civil Engineering, Brno University of Technology, Veveří 95, 602 00 Brno, tel. +420 54114 7368, e-mail: matesova.d@fce.vutbr.cz

which is based on the nonlinear fracture mechanics (NLFM) are introduced and subsequently combined with the spatial variation of concrete parameters reflecting the heterogeneous structure of concrete. Finally, the results of the analytical and numerical approaches are compared and a practical example is shown.

2. Formulation of the analytical model

The model presented here is a combination of analytical models proposed by Liu and Weyers (1998) and Li et al. (2006). As assumed in these models, concrete with an embedded reinforcing steel bar can be modeled as a thick-wall cylinder (Bažant, 1979; Pantazopoulou and Papoulia, 2001; Tepfers, 1979). This is shown schematically in fig. 1.

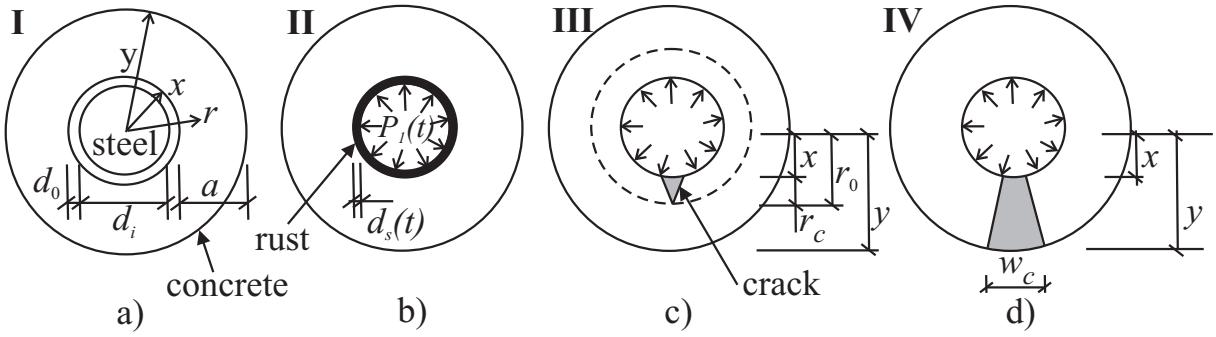

Figure 1: Scheme of the corrosion induced concrete cracking process; partially adopted from Li et al. (2006).

Four different stages of reinforcement corrosion propagation can be identified. Firstly, **stage I**, when no corrosion is present yet, is illustrated in fig. 1 a. Next, in **stage II**, the porous zone on the reinforcement-concrete interface is filled by corrosion products and the surrounding concrete eventually starts to be stressed due to corrosion (fig. 1 b). When the tangential stress in concrete exceeds its tensile strength, the crack initiates perpendicularly to the interface (fig. 1 c, **stage III**). After a certain time the crack propagates through the concrete cover (fig. 1 d) and we are able to measure the crack width on the concrete surface, **stage IV**.

Transition from stage I to stage II: To determine the time to corrosion initiation t_i, which is a transition time from stage I to stage II, we may use a wide spectrum of models for concrete carbonation or chloride ingress. The descriptions of those models is not the subject of this paper, see e.g. (Teplý et al., 2007). In the following text we assume t_i = 0.

Transition from stage II to stage III: A time to crack initiation, t_c [years] (fig. 1 c), which is a time of transition from stage II to stage III, can be estimated according to Liu and Weyers (1998) as:

$$t_\mathrm{c} = \frac{W_\mathrm{crit}^2}{2 \times 0.092 \left(\frac{1}{\alpha}\right) \pi \, d_\mathrm{i} \, i_\mathrm{corr}} \tag{1}$$

where d_i is the initial diameter of the reinforcement bar, i_corr is the corrosion current density [μA/cm^2], which is a measure of corrosion rate, α is a coefficient related to the type of corrosion products and W_crit is a critical amount of corrosion products that generate the critical tensile stresses and is defined as Liu and Weyers (1998):

$$W_{\mathrm{crit}} = \frac{\rho_{\mathrm{rust}} \pi \left[d_{\mathrm{i}} \left(d_{\mathrm{s,crit}} + d_0 \right) + 2 d_0 d_{\mathrm{s,crit}} \right]}{1 - \alpha \dfrac{\rho_{\mathrm{rust}}}{\rho_{\mathrm{st}}}} \tag{2}$$

where ρ_{rust} is the density of corrosion products, ρ_{st} is the density of steel, d_0 is the thickness of the annular layer of concrete pores (i.e. a pore band) at the interface between the bar and the concrete and $d_{\mathrm{s,crit}}$ is a critical thickness of a ring of corrosion products. Note, that in (Liu and Weyers, 1998) the term 2 d_0 d_{s} is neglected for W_{crit} derivation, which is not the case assumed here; $d_{\mathrm{s,crit}}$ is defined as:

$$d_{\mathrm{s,crit}} = \frac{a\, f_{\mathrm{t}}}{E_{\mathrm{ef}}} \left(\frac{x^2 + y^2}{x^2 - y^2} + \nu_c \right) \tag{3}$$

where a is a concrete cover, f_{t} is tensile strength of concrete, $E_{\mathrm{ef}} = E_{\mathrm{c}}/(1 + \varphi_{\mathrm{cr}})$ is an effective modulus of elasticity of concrete, E_{c} is elastic modulus of concrete, φ_{cr} is the creep coefficient of concrete, ν_c is a Poisson ratio, $x = (d_{\mathrm{i}} + 2d_0)/2$ and $y = a + (d_{\mathrm{i}} + 2d_0)/2$.

Transition from stage III to stage IV: Once the time t_{c} is reached, the crack starts to develop and we need to determine whether it has already propagated to the surface (fig. 1 d). The crack divides the thick-wall cylinder into 2 co-axial cylinders: inner cracked and outer uncracked ones, as shown in fig. 1 c. For the outer uncracked concrete cylinder, the theory of elasticity still applies. Let us assume that the cracks in the inner cracked concrete cylinder are smeared and uniformly circumferentially distributed, see fig. 4 a (Pantazopoulou and Papoulia, 2001) and that concrete is a quasibrittle material. According to Bažant and Jirásek (2002) and Noll (1972) there exists a residual cracked surface along the radial direction depending on the tangential strain of that point; it is a function of the radial coordinate r. It is assumed in this model that the residual tangential stiffness is constant along the cracked surface, i.e. in the interval $[x, r_0]$ and represented by $\alpha_{\mathrm{stiff}}\ E_{\mathrm{ef}}$, where α_{stiff} ($<$1) is the tangential stiffness reduction factor. According to Bažant and Planas (1998) the stiffness reduction factor α_{stiff} is dependent on the average tangential strain over the cracked surface ε_θ and can be determined as follows:

$$\alpha = \frac{f_{\mathrm{t}} \exp[-\gamma(\varepsilon_\theta - \varepsilon_\theta^c)]}{E_{\mathrm{ef}} \varepsilon_\theta} \tag{4}$$

where ε_θ^c denotes the average tangential cracking strain. After introduction of the constitutive relationship between radial and tangential stresses and strains (Pantazopoulou and Papoulia, 2001), the stress equilibrium (Fenner, 1989), boundary conditions for the concrete cylinder, and the continuity requirements and their combinations (see Li et al. (2006) for more details), we arrive at the following pair of nonlinear implicit equations:

$$0 = F_1 \left(\alpha_{\mathrm{stiff}}, r_0 \right) = f_{\mathrm{t}} - \frac{E_{\mathrm{ef}}}{1 - \nu_c^2} \left[\left(1 + \nu_c \right) c_1 \left(r_0 \right) + \frac{\left(1 - \nu_c \right) c_2 \left(r_0 \right)}{r_0^2} \right] \tag{5}$$

$$0 = F_2 \left(\alpha_{\mathrm{stiff}}, r_0 \right) = \frac{f_{\mathrm{t}} \exp \left(-\gamma k_2 \right)}{E_{\mathrm{ef}} k_1} - \alpha_{\mathrm{stiff}} \tag{6}$$

where

$$k_1 = \frac{\left(r_0^{\sqrt{\alpha_{\mathrm{stiff}}}} - x^{\sqrt{\alpha_{\mathrm{stiff}}}} \right) \left[c_3 \left(r_0 \right) + c_4 \left(r_0 \right) / \left(x r_0 \right)^{\sqrt{\alpha_{\mathrm{stiff}}}} \right]}{\sqrt{\alpha_{\mathrm{stiff}}} \left(r_0 - x \right)}$$

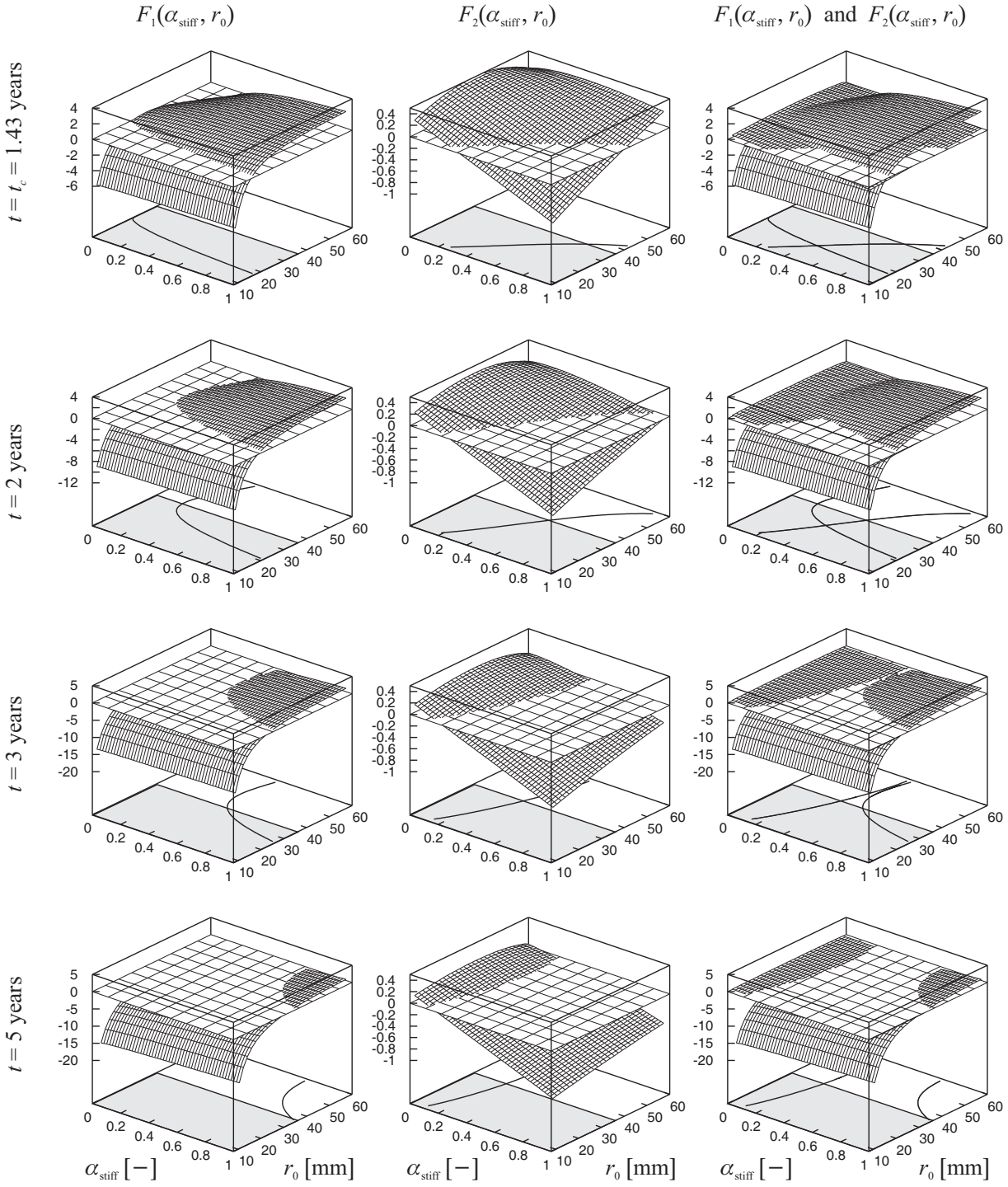

Figure 2: Evolution of functions $F_1(\alpha_{\text{stiff}}, r_0)$ and $F_2(\alpha_{\text{stiff}}, r_0)$ from eqs. (5) and (7) for various times t ($t_{\text{i}} = 0$).

$$k_2 \;=\; k_1 - \frac{1}{r_0 - x}\int_x^{r_0}\left(c_1(\xi) + \frac{c_2(\xi)}{\xi^2}\right)\mathrm{d}\xi$$

and where r_0 is the distance between the reinforcing bar center and a crack tip fig. 1 c and $c_1(r_0)$, $c_2(r_0)$, $c_3(r_0)$ and $c_4(r_0)$ are the coefficients depending on r_0. The definition of the functions is beyond the scope of this paper, see (Li et al., 2006). If a simultaneous solution to eqs. (5) and

(7), r_0 and α_{stiff} can be found in the intervals $r_0 \in (x,\ y)$ and $\alpha_{\text{stiff}} \in (0,\ 1)$, the crack has not propagated to the surface yet (the concrete is still in the stage III). We have programmed the solution of the problem and based on our experience, the Newton Rhapson scheme is successful in solving the set of nonlinear equations. A good starting point for the solver is the middle point of the intervals: r_0 = (x + y) / 2 and α_{stiff} = 0.5. In case that the solution cannot be found in the identified ranges of r_0 and α_{stiff}, the crack already penetrated to the surface. By substituting $r_0 \rightarrow y$ in eqs. (5) and (7) we obtain a new set of nonlinear equations. Their simultaneous solution leads to finding α_{stiff} (stiffness reduction coefficient) that is needed for the computation of the crack width w_{c}:

$$w_{\text{c}} = \frac{4\pi d_{\text{s}}(t)}{(1-\nu_c)(x/y)^{\sqrt{\alpha_{\text{stiff}}}} + (1+\nu_c)(y/x)^{\sqrt{\alpha_{\text{stiff}}}}} - \frac{2\pi y f_{\text{t}}}{E_{\text{ef}}} \tag{7}$$

where $d_{\text{s}}\ (t)$ is the thickness of a ring of corrosion products (fig. 1 b) that can be determined from:

$$d_{\text{s}} = \frac{W_{\text{rust}}\ (t)\left(1 - \alpha\dfrac{\rho_{\text{rust}}}{\rho_{\text{st}}}\right) - \pi\rho_{\text{rust}} d_{\text{i}} d_0}{\pi\rho_{\text{rust}}(d_{\text{i}} + 2d_0)} \tag{8}$$

where $W_{\text{rust}}(t)$ is the mass of corrosion products. Note, that d_{s} is not correctly derived in Li et al. (2006) and that is why our eq. (8) differs from theirs. Obviously, $W_{\text{rust}}(t)$ increases with time and according to Liu and Weyers (1998) can be determined from:

$$W_{\text{rust}}(t) = \sqrt{\frac{2 \times 0.092\pi a}{\alpha} \int_{t_{\text{i}}}^{t} i_{\text{corr}}\ (t)\ \mathrm{d}t} \tag{9}$$

The most complicated part of the approach is the solution of functions $F_1(\alpha_{\text{stiff}},\ r_0)$ and $F_2(\alpha_{\text{stiff}},\ r_0)$. We help the reader to imagine how the two implicit functions look by plotting their evolution with time in fig. 2. For the time range of $\langle 1.43,\ 2.8\rangle$, the simultaneous solution $F_1(\alpha_{\text{stiff}},\ r_0)$ = 0 and $F_2(\alpha_{\text{stiff}},\ r_0)$ = 0 exists within the above identified ranges of α_{stiff} and r_0 (stage III). The solution is illustrated by the intersection of two curves in the base. Upon reaching the time of years, the crack width becomes nonzero (stage IV).

3. Numerical model

ATENA program (Červenka and Pukl, 2005) was used for the simulation of a nonlinear response of the corroded reinforcement in concrete. For modeling of a nonlinear behavior a material constitutive model based on a smeared approach that can successfully describe the discrete crack propagation was applied. In particular, we used the fracture-plastic model named NLCEM in ATENA program. Concrete with reinforcement was modeled as a 2D problem and in accordance to the definition of an analytical model; thick-wall cylinder geometry was modeled (see fig. 1 a). The dimensions are: a = 30 mm and d_{i} = 20 mm. The thickness of the annular layer of concrete pores d_0 was ignored, because this thickness is only important for the time analysis; it delays stress development (this void space is firstly filled by the corrosion products). Expansion of corrosion products was simulated by application of (negative) shrinkage of the reinforcement elements.

3.1. Deterministic model

At first the system was treated as the deterministic to study the damage mechanisms and the development of stresses and cracks. Two extreme cases of boundary conditions were studied: without circuit restraint of the outer concrete face (free margins) and with a circuit restraint by applying the fixed hinge supports around the concrete face (see e.g. fig. 4 a,d for illustration of boundary conditions). The major input parameters of the concrete constitutive law were: modulus of elasticity E = 30.32 GPa, compressive strength f_{c} = 25.5 MPa, tensile strength f_{t} = 2.317 MPa and fracture energy G_{F} = 57.93 N/m. During the numerical calculations, we have monitored several important variables: the radial displacement d at the steel–concrete interface and stresses at three positions of concrete: (1) interface with steel, (2) the middle of concrete layer thickness and (3) outer concrete boundary. Two types of stresses were monitored at the three positions: the radial and tangential stresses σ_{r} and σ_{τ}. Their dependence on the on the displacement d is plotted in fig. 3 for both free and restraint boundary conditions.

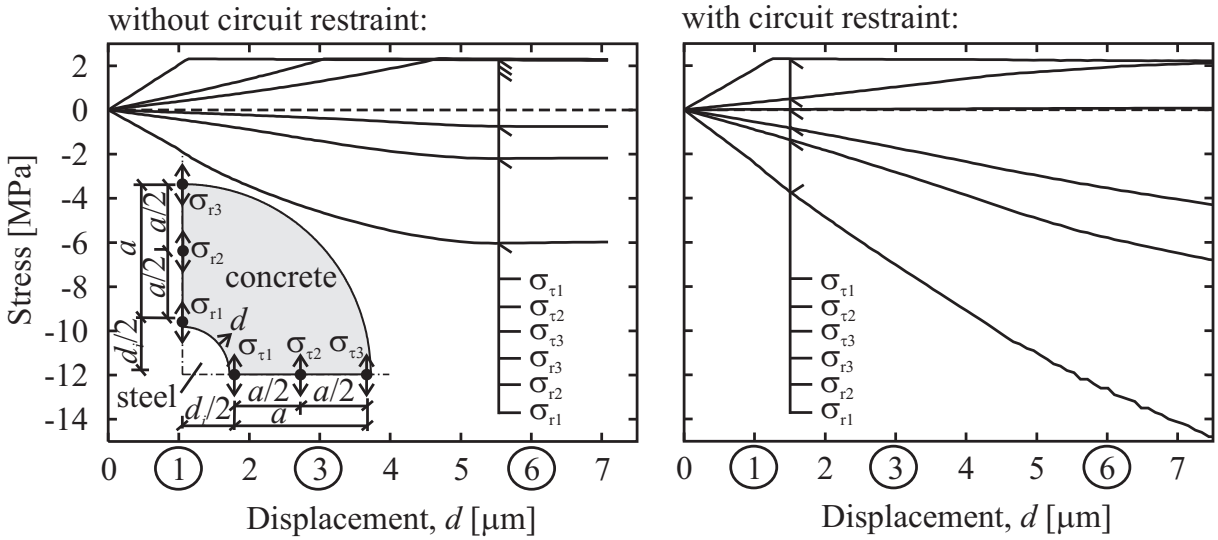

Figure 3: Deterministic solution of the numerical models; comparison of restrained and non restrained boundary conditions at outer concrete boundary.

For a detailed analysis of stress profiles in concrete presented in fig. 4, three stages of crack development were chosen coinciding with $d = \ 1, 3$ and 6 m (circled values from fig. 3). The first stage (d = 1 m) is characterized by crack initiation from the interface for both free and restrained circuit boundary conditions; the peak tangential stress $\sigma_{\tau 1}$ equals the tensile concrete strength. In the case of free boundary conditions, the radial and tangential stresses differ only in the sign (as can be easily predicted by a simple analytical computation), while in the case of restraint boundaries, a small pressure can be identified perpendicular to the outer concrete interface. The second and third stages record gradual crack growth; the cracks growth is suppressed by the constraint in the bottom raw of fig. 4.

3.2. Stochastic model

The uniform and rotationally symmetric crack distribution from fig. 4 is not very realistic. In order to simulate the heterogeneous structure of concrete, the spatial variability of material was modeled by modifications of chosen input values of concrete. In reality, the concrete does not

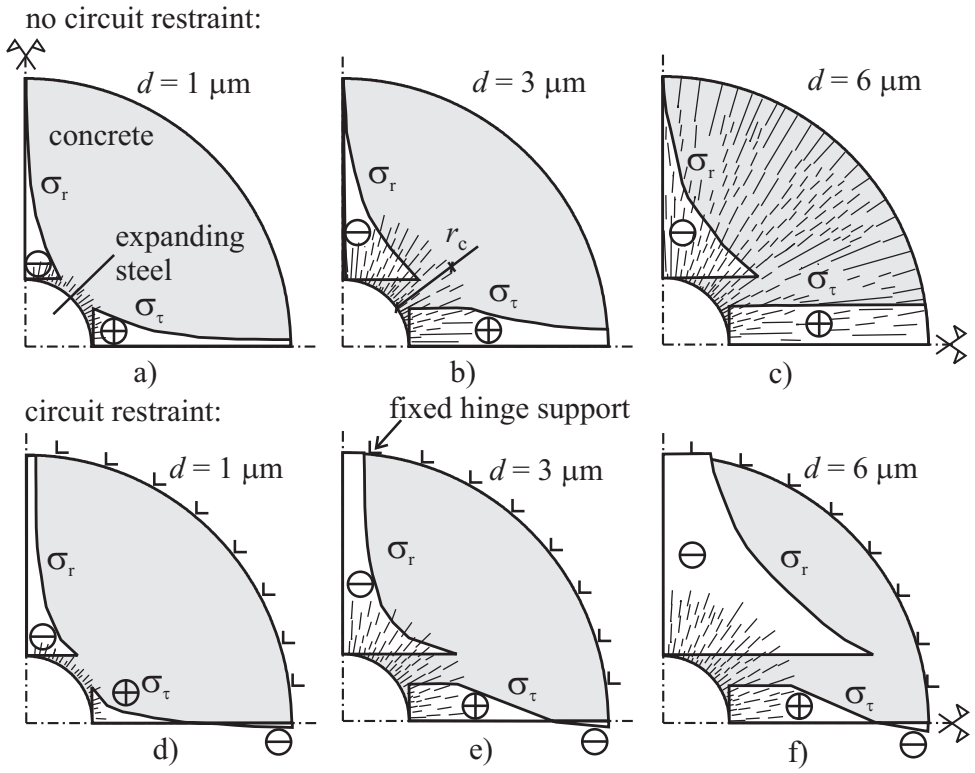

Figure 4: Tangential and radial stresses development and cracks distribution in concrete cover.

have uniform properties over its volume and this can be suitably modeled by random fields of the concrete parameters. We remark, that such an approach automatically disturb the rotational stress symmetry and introduce damage initialization similarly to the real situation.

Two parameters of the constitutive law of concrete were selected to be randomized and they were studied separately. Namely, the modulus of elasticity E and the tensile strength f_{t} were randomized to trigger fracturing. The applied random fields were normally distributed with coefficient of variation 30% and 20% respectively. The mean value was taken from the deterministic analyses (section 3.1) to obtain consistent results. One of the most important property of a random field is the autocorrelation structure defined through the autocorrelation function and the autocorrelation length. Briefly, the autocorrelation length is a parameter controlling the rate of spatial variability of the parameter; see (Vořechovský, 2004, 2005) for details on random field modeling. In our analysis, the correlation lengths of 0.01 m were assumed in both directions together with a squared exponential autocorrelation function (isotropic correlation structure of the field). The autocorrelation length roughly coincides with the maximum aggregate size of concrete. For illustration of the random field and the rate of fluctuation, see fig. 5.

The results of the stochastic nonlinear calculations are visualized through the dependence of tangential stress $\sigma_{\tau 1}$ on the radial extension of steel (displacement d), see diagrams in fig. 6. As can be seen, the randomization of the local E modulus does not affect the crack initiation stress (which still equals the concrete tensile strength) while the randomized strength influences the crack initiation stress while not affecting the initial overall stiffness. We remark, that due to the relatively small dimensions of concrete material with respect to the concrete dimensions, the fracture is very ductile and therefore the mechanism is closer to the parallel coupling of

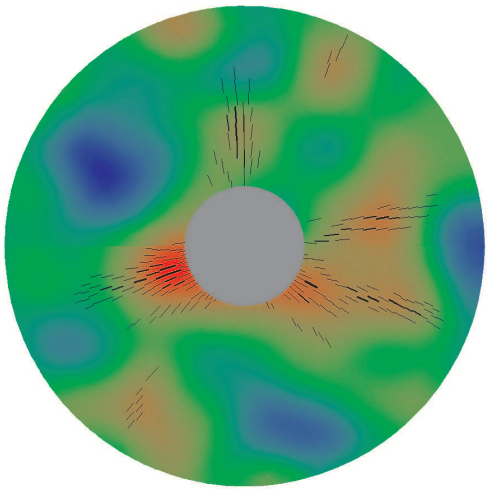

Figure 5: Realization of a random field of local tensile strength f_{t} and cracks developed in the post peak stage of $\sigma_{\tau 1}$. The colors illustrate the tensile strength distribution from the lowest to the greatest values (from red through green to blue, respectively).

micro-bonds rather than a weakest link principle, see (Vořechovský, 2004) for details.

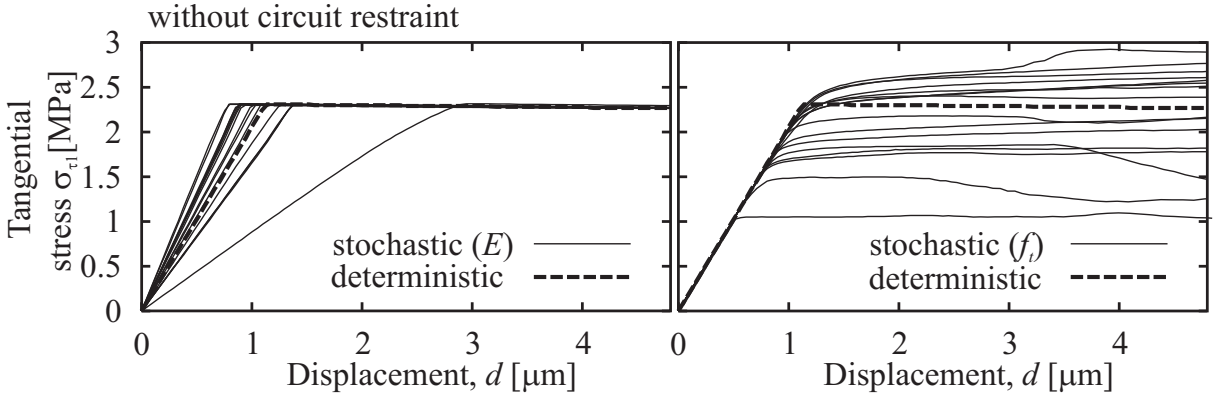

Figure 6: Results of nonlinear stochastic simulations; comparison of spatial variability applied to modulus of elasticity E and tensile strength f_{t} of concrete.

4. Comparison of analytical and numerical models

The comparison of both models was performed at the deterministic level. The numerical model without circuit boundary conditions was used as it coincides with the formulation of the analytical model. The comparison of both models was done through the crack development quantified by coordinate r_{c}, see fig. 1 c and 4 c. The parameters identical for both numerical and analytical approaches are: $d_{\mathrm{i}} = 20$ mm, $d_0 = 0$ mm, a = 30 mm, f_{t} = 2.317 MPa, E_{ef} = E = 30.32 GPa and ν_c = 0.2. The trend of crack length r_{c} in dependence on the displacement d is plotted in fig. 7 together with tangential stresses obtained from numerical calculations. Note, that the displacement d monitored during numerical calculations does not coincide with the thickness of a ring of corrosion products d_{s} that is featured in the analytical approach. The measure of displacement d does not take into account the loss of steel due to rust production. For the purpose

of the comparison of both models, d_s was recalculated to d through the steel and rust densities considered as ρ_{rust} = 3600 kg/m^3 and ρ_{st} = 7850 kg/m^3 by realizing that the total weight of both materials must be kept constant. The growth of d_s (or d) is related to the time (see eqs. 8 and 9); this relation depends mainly on the current density i_{corr}. A detailed time analysis is beyond the scope of this paper; only the nonlinear trend of d in time is sketched in the right bottom of fig. 7. Obviously, in the deterministic case, both models are comparable. However, the numerical model is much more flexible and its predictive capabilities are higher as it can easily accommodate advanced features such as the spatial variability of material parameters or more complex geometries. The latter becomes important when analyzing real-life examples as the one presented in the following section.

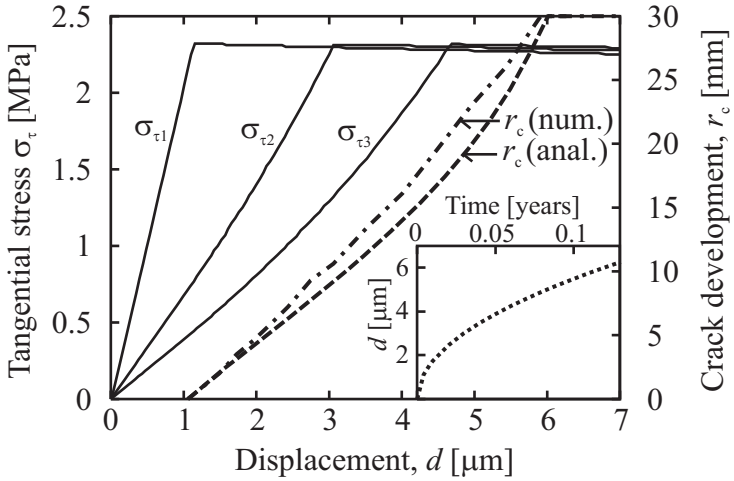

Figure 7: Comparison of analytical and numerical model through the crack length r_c together with tangential stresses obtained from numerical simulation. Time dependence of d is sketched in right bottom.

5. Practical application

The thick wall cylinder geometry around the steel reinforcement is not a usual geometry of a real structure. To illustrate the real danger of steel corrosion in reinforced concrete girder, we prepared a model of its lower part together with four reinforcing bars (20 mm thick) and concrete cover of 40 mm. A uniform type of corrosion and the same corrosion rate for all four reinforcing bars were assumed. The crack development in concrete due to rust products of steel as predicted by the numerical model is sketched in fig. 8. Note that in reality, opening of crack accelerates the corrosion progress because of easier transport of oxygen and water. The crack patterns agree well with the damage observed in real structures.

6. Conclusions

The application of analytical and numerical approaches to simulation of concrete cracking due to corrosion of reinforcement was presented. At first, a combination and detailed analysis of the two analytical models proposed by Liu and Weyers (1998) and Li et al. (2006) was described. Four distinct phases of the corrosion process are identified and the process is modeled by numerical computations obtained with the nonlinear finite element code. The numerical model

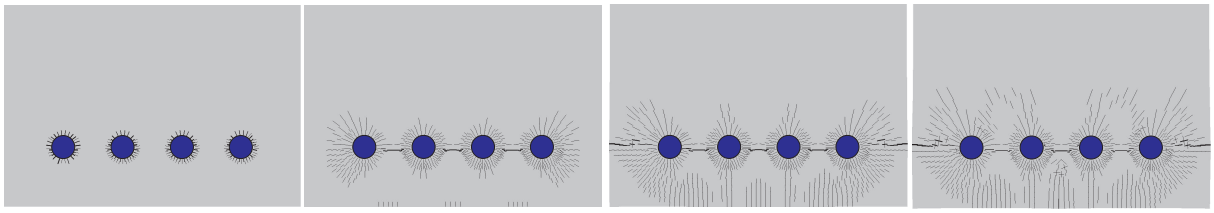

Figure 8: Crack development due to corrosion in reinforced concrete beam.

features the state-of-the-art in nonlinear fracture mechanics and the heterogeneous structure of concrete is shown to be modeled via spatially varying parameters of the constitutive law. These results are of high importance in durability based design of structures.

7. Acknowledgement

This outcome has been achieved with the financial support of the Ministry of Education, Youth and Sports, project No. 1M0579, within activities of the CIDEAS research centre. In this undertaking, theoretical results gained in the project GACR 103/06/P086 were partially exploited.

References

Bažant, Z. P. (1979). Physical model for steel corrosion in concrete sea structures - theory. *Journal of Structural Division 105*(ST6), 1137–1153.

Bažant, Z. P. and M. Jirásek (2002). Nonlocal integral formulations of plasticity and damage: Survey and progress. *Journal of Engineering Mechanics 128*(11), 1119–1149.

Bažant, Z. P. and J. Planas (1998). *Fracture and Size Effect in Concrete and Other Quasibrittle Materials*. CRC Press, Boca Raton and London.

Fenner, R. T. (1989). *Mechanics of Solids*. Oxford: Blackwell Scientific Publications.

Li, C. Q., R. E. Melchers, and J. J. Zheng (2006). An analytical model for corrosion induced crack width in reinforced concrete structures. *ACI Structural Journal 103*(4), 479–482.

Liu, Y. and R. E. Weyers (1998). Modeling the time-to-corrosion cracking in chloride contamined reinforced concrete structures. *ACI Material Journal 95*(6), 675–681.

Noll, W. (1972). A new mathematical theory of simple materials. *Arch. Ration. Mech. Anal. 48*, 1–50.

Pantazopoulou, S. J. and K. D. Papoulia (2001). Modeling cover-cracking due to reinforcement corrosion in rc structures. *Journal of Engineering Mechanics 127*(4), 342–351.

Tepfers, R. (1979). Cracking of concrete cover along anchored deformed reinforcing bars. *Magazine of Concrete Research 31*(106), 3–12.

Teplý, B.and Matesová, D., Chromá, and P. M., Rovnaník (2007). Stochastic degradation models for durability limit state evaluaton: SARA – Part VI. In *3rd International Conference on Structural Health Monitoring of Intelligent Infrastructure*, Vancouver, Canada, to appear.

Červenka, V. and R. Pukl (2005). Atena program documentation. Technical report, Červenka Consulting, Prague, Czech Republic. http://www.cervenka.cz.

Vořechovský, M. (2004). *Stochastic fracture mechanics and size effect*. Ph. D. thesis, Brno University of Technology, Brno, Czech Republic.

Vořechovský, M. (2005). Simulation of cross correlated random fields by series expansion methods. *Structural safety*, in review.